RSC Advances

PAPER

View Article Online
View Journal | View Issue

Cite this: *RSC Adv.*, 2020, **10**, 18553

Synthesis, crystal structure and antiproliferative mechanisms of gallium(III) complexes with benzoylpyridine thiosemicarbazones†

Jinxu Qi,[ab] Taichen Liu,[b] Wei Zhao,[b] Xinhua Zheng*[b] and Yihong Wang*[a]

Received 31st March 2020
Accepted 1st May 2020

DOI: 10.1039/d0ra02913k

rsc.li/rsc-advances

We have prepared six thiosemicarbazone ligands and synthesized the corresponding Ga(III) complexes. The antitumor activity of the ligand increases with its lipophilicity, and the antitumor activity of the Ga(III) complexes is affected by the ligands. Since **C6** has the highest anticancer proliferative activity (0.14 ± 0.01 μM) against HepG-2 (Human hepatocarcinoma cell line), we characterized its structure by X-ray single crystal diffraction and explored its antiproliferation mechanism. Anti-tumor mechanism results show that Ga(III) complex (**C6**) promoted HepG-2 cell cycle arrest in the G1 phase by regulating the expression of cell cycle-associated proteins (Cdk 2, cyclin A and cyclin E). Ga(III) complex (**C6**) promotes apoptosis by consuming intracellular iron, enhancing intracellular reactive oxygen species (ROS), activating caspase-3/9, releasing cytochromes and apoptotic protease activating factor-1 (apaf-1).

Introduction

Gallium nitrate was introduced into clinical trials in the 1980s due to its good anticancer potential.[1] Ga(III) complexes are important anti-tumor drugs that are superior to platinum due to certain aspects of their biological effects.[2–6] Reports on the detection of poly-phosphates using Ga(III) complexes indicate that gallium has a strong binding affinity for ATP.[7,8] Therefore, Ga(III) complexes may have the potential to inhibit ATP. Similar to iron, Ga(III) enters cells by binding to transferrin, so the solution to increase activity is to increase the bioavailability of Ga.[9–11] The ligand-modified Ga(III) complexes exhibit advantageous pharmaceutical properties in various aspects, such as pharmacokinetics, affinity for malignant cells, and anti-tumor proliferative effect.[12–14] Ga(III) complexes induce apoptosis in cancer cells by activating caspase activity and modulating cyclin to inhibit the cell cycle.[15–18]

The complexation of Ga(III) with thiosemicarbazone enhances the biological activity of Ga(III) and is considered to be an important strategy for the development of cytotoxic drugs.[10,18–20] Lipophilicity plays a leading role in the rate at which molecules enter cells, and complexation can increase the lipophilicity of Ga(III).[21] At the same time, the biological activity of thiosemicarbazone is closely related to the ability of forming complex with the metal and the lipophilicity of the molecule.[21–24] Triapine (3-aminopyridine-2-carboxaldehyde thiosemicarbazone) is a potent ribonucleotide reductase inhibitor and is the most prominent representative of this family.[25–27] It is currently used in phase I and phase II clinical trials for a variety of malignancies.[25] Another star molecule (di-2-pyridylketone 4-cyclohexyl-4-methyl-3-thiosemicarbazone, DPC) has entered clinical trials for drug-resistant cancer treatment in 2016.[28] The synthesis and application of thiosemicarbazone and its gallium complex have been paid attention to and become one of the most promising research fields.

In order to further improve the anti-tumor mechanism of thiosemicarbazone-Ga(III) complexes, the following studies were carried out: (1) six thiosemicarbazone ligands and their corresponding Ga(III) complexes are synthesized (Scheme 1); (2) the structure and activity relationships of these compounds have been studied; (3) intracellular ROS, mitochondrial membrane potential, caspase-3/9 activation, and expression of cyt-c and apaf-1 were analyzed and used to investigate the mechanism behind gallium complexes promoted apoptosis; (4) expression of cell cycle-associated proteins (cdk2, cyclin A, cyclin E) which

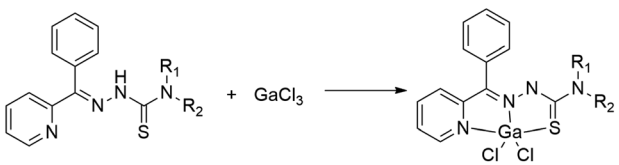

L1: R_1 = H, R_2 = H; L4: R_1 = cyclohexyl, R_2 = H;
L2: R_1 = Me, R_2 = H; L5: R_1 = Me, R_2 = Me;
L3: R_1 = Et, R_2 = H; L6: R_1 = Me, R_2 = cyclohexyl;

Scheme 1 Synthetic route of Ga(III) complexes.

[a]*School of Chemistry and Chemical Engineering, Southeast University, Nanjing 211189, China*

[b]*School of Medicine, Pingdingshan University, Pingdingshan, China*

† Electronic supplementary information (ESI) available. CCDC 1899688. For ESI and crystallographic data in CIF or other electronic format see DOI: 10.1039/d0ra02913k

are also related with the apoptosis process, was further examined to better understand the underlying mechanism.

Results and discussion

Synthesis and crystal structure description

The thiosemicarbazone ligands (**L1–L6**) were prepared as described in the literature, and the prepared ligands were subjected to NMR, mass spectrometry and elemental analysis. Coordination of an equimolar amount of ligand with Ga(III) chloride to synthesize a series of 1 : 1 ligand/Ga(III) complexes, and products were crystallized from methanol in high purity without purification (Scheme 1). The crystal data of **C6** was displayed in Table S1,† and the selected angles and bond lengths are listed in Table S1.† **C6** crystallized in the monoclinic system, and space group $P2_1/n$. The Ga(III) metal center of **C6** is coordinated by one S atoms, two Cl atoms (Cl1 and Cl2) and two N atoms (N1 and N2), which formed a deformed trigonal bipyramid (Fig. 1). The lengths of Ga1–N1 [2.098(2) Å] and Ga1–N2 [2.0581(17) Å] are similar. There is no significant difference between the length of Ga1–Cl1 [2.2264(7) Å] and Ga1–Cl2 [2.2070(7) Å] bonds. The Ga–Cl and Ga–N bonds were shorter than the length of Ga1–S1 [2.3291(7) Å]. In Ga(III) complex, the anion Cl and tridentate thiosemicarbazone coordinate with the central copper ion(II) to form an approximately planar structure. The bond angles and bond lengths in **C6** are identical to other known compounds in published articles.[10,11,29]

Anticancer properties of Ga(III) complexes

A liver hepatocellular carcinoma cell line (HepG-2) was used to evaluate the anticancer activity of the thiosemicarbazide ligand and the Ga(III) complexes. All of the thiosemicarbazide ligands (**L1–L6**) and Ga(III) complexes (**C1–C6**) showed potent antiproliferative activity and results were listed in Table 1. The anticancer activity of $GaCl_3$ (50 μM) was not observed. More importantly, these chemical agents showed very low toxicity to normal cells (LO-2) compared to tumor cells.

As shown in Table 1, the anticancer activity of **L1–L6** increased sequentially after HepG-2 cells were treated for 48 hours. Among them, the antiproliferative activity of **L1** (IC_{50}, 11.35 ± 0.21 μM) is effectively lower than that of **L6** (IC_{50}, 0.32 ± 0.02 μM). Similarly, the cytotoxicity of the Ga(III) complex increased synchronously with ligand numbers after 48 hours of treatment on HepG-2. These data indicate that the antiproliferative activity of Ga(III) complexes is determined by the corresponding ligand, and the anticancer activity of the ligand is enhanced by coordination with gallium. **L6** (IC_{50}, 0.32 ± 0.02 μM) and **C6** (IC_{50}, 0.14 ± 0.01 μM) has the most excellent antiproliferative activity against HepG-2 in ligands and complexes, respectively. After 48 h of treatment, the cytotoxicity of **L1–L6** increases in turn, and the toxicity of the complex is higher than that of the corresponding ligand. However, **L6** has the best selectivity indices (SI) in ligands, and the presence of Ga(III) has a better impact on this parameter. The antitumor activity of all Ga(III) complexes was higher than that of cisplatin.

Table 1 IC_{50} values of ligands and Ga(III) complexes toward cell lines for 48 h

	IC_{50} (μM)		
	HepG-2	LO2	SI
L1	11.35 ± 0.21	43.64 ± 2.84	3.84
L2	4.56 ± 0.11	35.75 ± 2.19	7.84
L3	2.43 ± 0.10	32.97 ± 3.64	13.57
L4	1.32 ± 0.09	30.32 ± 2.16	22.97
L5	0.57 ± 0.04	23.85 ± 2.00	41.84
L6	0.32 ± 0.02	11.54 ± 0.54	36.06
C1	5.75 ± 0.54	33.76 ± 2.13	5.87
C2	2.76 ± 0.39	25.83 ± 2.93	9.36
C3	1.23 ± 0.09	26.64 ± 3.86	21.66
C4	0.97 ± 0.02	20.43 ± 1.13	21.06
C5	0.34 ± 0.02	18.86 ± 1.64	55.47
C6	0.14 ± 0.01	10.65 ± 1.69	76.07
Cisplatin	22.43 ± 2.21	21.27 ± 2.35	—
$GaCl_3$	>50	>50	—

Cell apoptosis assay

Apoptosis is physiological and programmed death process, a basic biological phenomenon of cells.[30–32] Lack of apoptosis in cell proliferation is a crucial factor in tumor development.[33–35] Therefore, an effective way to treat tumors is to stimulate and restore apoptosis of tumor cells. To assess the effect of concentration on the ability of gallium complexes (**C6**) to promote apoptosis in HepG-2 cells, Annexin v-fitc/PI was used to stain the cells and flow cytometry was used to

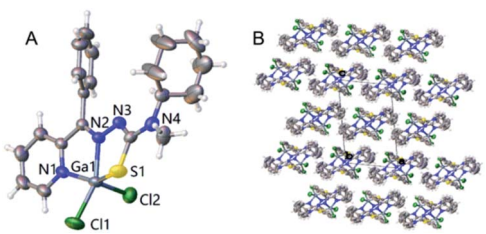

Fig. 1 (A) A molecular structure of **C6** showing the environment about the Ga(III) atom. (B) The pack of Crystal.

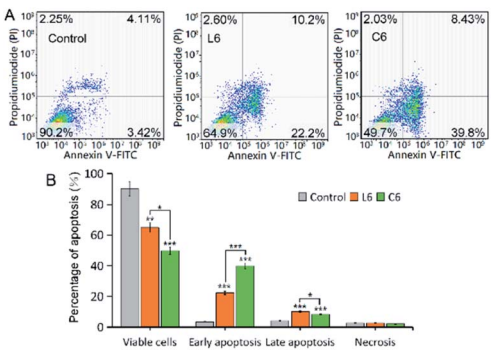

Fig. 2 (A) Representative dot plots of PI and Annexin V double staining on the HepG-2 cells; (B) comparison of apoptosis distributions.

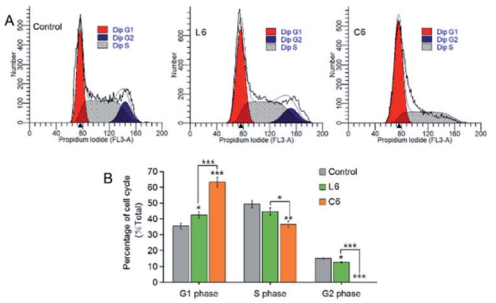

Fig. 3 (A) Effect on the cell cycle of the HepG-2 cells; (B) comparison of cell cycle distributions.

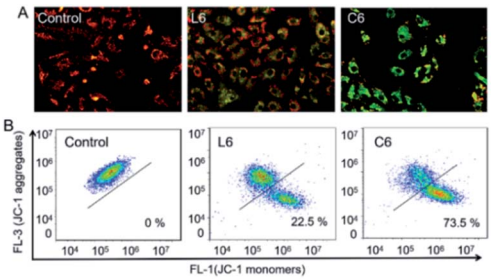

Fig. 4 Assay of HepG-2 cells mitochondrial membrane potential with JC-1 as fluorescence indicator. (A) Observed with a fluorescent inverted microscope; (B) examined by flow cytometry.

detect apoptosis (Fig. 2). After incubation for 24 hours at 5 μM of **L6** and **C6**, the percentage of early apoptosis and late apoptosis increased to 24.87% and 40.7% relative to the control.

Cell cycle analysis

We used flow cytometry to evaluate the effect of thiosemicarbazide ligands and Ga(III) complexes on cell cycle, and propidium iodide (PI) was used to stain DNA of HepG-2 cells as well as the cell cycle distribution was performed by flow cytometry (Fig. 3). After 24 h of co-cultivation of **L6** and **C6** with the cells, quantification of the results showed that the percentage of G2 phase cells were reduced compared to the vehicle-treated control. The increase in G1 phase cell proportion was consistent with other data.

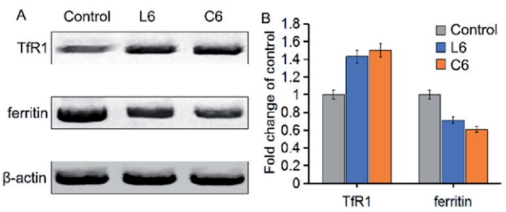

Fig. 5 (A) Western blot analysis of TfR1 and ferritin proteins in HepG-2 cells treated with 5 μM of **L6** and **C6** for 24 h; β-actin was used as the internal control. (B) Expression levels of TfR1 and ferritin proteins shown as percentages; the values are relative to the control.

Mitochondrial membrane potential assay

Mitochondria are the main site for cellular aerobic respiration, known as "power house", and the dissipation of mitochondrial membrane potential may be one of the causes of cell apoptosis.[36] To examine the effect of the ligands and Ga(III) complexes on mitochondrial membrane potential ($\Delta\psi_m$), changes in mitochondrial membrane potential were monitored by flow cytometry using JC-1 fluorescent probe (5,5,6,6′-tetrachloro-1,1′,3,3′-tetraethyl-imidacarbocyanineiodide). Red fluorescence (JC-1 aggregates) occurs when the mitochondrial membrane potential is high, whereas green fluorescence (JC-1 monomer) is observed when the mitochondrial membrane potential is low (Fig. 4A). HepG-2 was cultured with 5 μM of **L6** and **C6**, the $\Delta\psi_m$ was significantly ($p < 0.001$) decrease to 22.5% and 73.5% relative to the control, respectively.

The expression of transferrin receptor-1 (TfR1) and ferritin proteins affected by Ga(III) complex

To further investigate the effects of thiosemicarbazone and gallium ions on iron metabolism in cells, we tested the effects of **L6** and **C6** on ferritin and transferrin receptor-1 (TfR1) expression (Fig. 5). After 24 h of co-cultivation of **L6** and **C6** with the cells, quantification of the results showed that the expression of TfR1 were increased by about 1.43 fold and 1.50 fold compared to the vehicle-treated control. While the expression of ferritin reduced 0.72 fold and 0.61 fold relative to the control group. Both ligand and Ga(III) complex down-regulated ferritin expression and up-regulated TfR1 expression, indicating cell response to iron consumption. The results on TfR1 and ferritin expression being very similar for the Ga(III) complex **C6** and the corresponding ligand **L6** could suggest that in both cases the ligand can chelate iron which would mean that an exchange between gallium and iron occurs (Fig. 5).

Intracellular ROS measurements

The loss of mitochondrial function may cause disorder of anti-free radical metabolism and free radical oxidative metabolism in cells.[37] Drug invasion leads to excessive intracellular reactive oxygen species (ROS) production or decreased clearance capacity, resulting in oxidative stress and apoptosis.[38] After incubation for 24 hours at 5 μM of **L6** and **C6**, the percentage of intracellular ROS level increased to 17.12% and 27.12% relative to the control (Fig. 6). At the same concentration, **C6** promoted the ability of HepG-2 cells to produce ROS significantly stronger than (Fig. 6) **L6**.

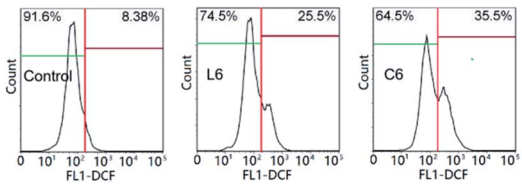

Fig. 6 The intracellular reactive oxygen species (ROS) of HepG-2 cells.

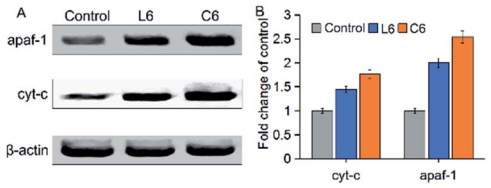

Fig. 7 (A) Western blot was used to determine the protein levels of apaf-1 and cyt-c; (B) densitometric analysis of apaf-1 and cyt-c: the density of each protein bands was normalized with that of the β-actin band shown in part A.

Detection of changes in protein levels of apaf-1 and cyt-c

The apoptotic active substances (cyt-c) will release from the mitochondria through the permeability transition (PT) pore under the action of the mitochondrial membrane potential ($\Delta\psi_m$).[39,40] To confirm this phenomenon, the influence of **L6** and **C6** on the expression of apaf-1 and cyt-c in HepG-2 cells were performed by western blot (Fig. 7). The results showed that 5 μM of **L6** had significant effect on the expression of apaf-1 and cyt-c. After treated with 5 μM **C6**, induced a significant ($p < 0.05$) increase in apaf-1 and cyt-c protein levels than **L6** incubated cells. The increase in pro-apoptotic protein levels implied the occurrence of apoptosis.

Caspase-3/9 activation assay

Upon initiation of apoptosis, cyt-c is released into the cytoplasm and subsequently activates caspase-3/9 protein to form apoptotic bodies.[41–43] Thus, the percentage of activated caspase-3/9 was analyzed when HepG-2 cells were treated with **L6** and **C6**, respectively (Fig. 8). After incubation with 5 μM of **L6** and **C6** for 24 hours, the percentage of activated caspase-3 protein level increased to 10.6% and 24.4% compared to the control, and the activated caspase-9 protein level increased to 8.2% and 17%. The results showed that **L6** and **C6** are potent activators of caspase-3/9, and up-regulation of these pro-apoptotic protein is an important pathway for apoptosis of HepG-2 cells induced by thiosemicarbazide ligands and their gallium complexes.

Detection of changes in protein levels of cell cycle related proteins

Regulation of the cell cycle is influenced by cyclin, cyclin-dependent kinase (Cdk), Cdk inhibitor, DNA, and the core

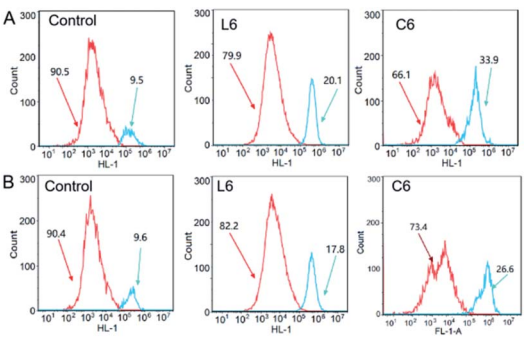

Fig. 8 (A) The activation of caspase-3 in HepG-2 cells; (B) the activation of caspase-9 in HepG-2 cells.

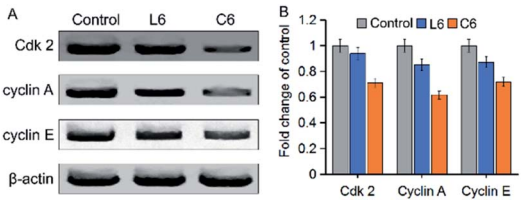

Fig. 9 (A) Western blot was used to determine the protein levels of Cdk 2, cyclin A and cyclin E in HepG-2 cells; (B) densitometric analysis of Cdk 2, cyclin A and cyclin E: the density of each of these protein bands was normalized with that of the β-actin band shown in part A.

mechanism is the activation and regulation of Cdk inhibitors.[44] Therefore, **L6** and **C6** treated cells were analyzed to reveal the cyclin-dependent kinases (Cdk 2) and cyclins (cyclin A and cyclin E) expression (Fig. 9). HepG-2 cells treated with 5 μM **L6** and **C6** induced significant ($p < 0.05$) decreased in these proteins' expression level.

Experimental

Material

Chemicals and solvents were purchased from Innochem Co., Ltd. (Shanghai, China), all of which are of analytical grade and used without further purification. Deionized water was used throughout the experiment. The HepG-2 and LO2 cell lines were obtained from Chinese Academy of Sciences. At 298 K, NMR spectra were recorded on a Bruker AVANCE III HD 600 MHz spectrometer. Proton chemical shifts were referenced to the central peak of DMSO-d_6. Electrospray ionization mass (ESI-MS) spectrometry were performed on an Agilent 1260-6224 ion trap spectrometer, working in aqueous solution.

Synthesis and characterization of ligands (L1–L6)

The synthesis of ligands (**L1–L6**) was performed by previous methods.[11] One mole equivalent of 2-benzoyl pyridine and 5 drops of CH_3COOH were added to 10 mL ethanol (1 mM) solution of thiosemicarbazide and refluxed for 4 h. The formed precipitate was collected by filtration and washed with ethanol, and dried *in vacuo*. 2-(Phenyl(pyridin-2-yl)methylene)hydrazinecarbothioamide (**L1**) and *N*,*N*-dimethyl-2-(phenyl(pyridin-2-yl)methylene)hydrazinecarbothioamide (**L5**) have been reported in our previous literature.[15,20]

***N*-Methyl-2-(phenyl(pyridin-2-yl)methylene)hydrazinecarbothioamide (L2).** Yield 69%. *Anal. Calcd* for $C_{14}H_{14}N_4S$: C, 62.20; H, 5.22; N, 20.72. Found: C, 62.34; H, 5.20; N, 20.76. ^{1}H NMR (600 MHz, DMSO-d_6) δ 12.83 (s, 1H), 8.87 (ddd, $J = 5.0$, 1.7, 0.9 Hz, 1H), 8.73 (d, $J = 4.7$ Hz, 1H), 8.02 (td, $J = 7.8$, 1.8 Hz, 1H), 7.66–7.63 (m, 2H), 7.61 (ddd, $J = 7.7$, 4.9, 1.1 Hz, 1H), 7.49–7.44 (m, 3H), 7.36 (dd, $J = 8.0$, 1.0 Hz, 1H), 3.05 (d, $J = 4.6$ Hz, 3H). MS *m*/*z* (%) 269.09 (M − H, 100).

***N*-Ethyl-2-(phenyl(pyridin-2-yl)methylene)hydrazinecarbothioamide (L3).** Yield 76%. *Anal. Calcd* for $C_{15}H_{16}N_4S$: C, 63.35; H, 5.67; N, 19.70. Found: C, 63.39; H, 5.61; N, 19.66. ^{1}H NMR (600 MHz, DMSO-d_6) δ 12.76 (s, 1H), 8.87 (ddd, $J = 4.9$, 1.8, 0.9 Hz, 1H), 8.78 (s, 1H), 8.02 (td, $J = 7.8$, 1.8 Hz, 1H), 7.65–7.63 (m, 2H), 7.61 (ddd, $J = 7.7$, 4.9, 1.1 Hz, 1H), 7.48

(qd, J = 3.1, 1.2 Hz, 3H), 7.35 (dt, J = 8.1, 1.1 Hz, 1H), 3.62 (dd, J = 7.2, 6.1 Hz, 2H), 1.15 (t, J = 7.1 Hz, 3H). MS m/z (%) 283.11 (M − H, 100).

***N*-Cyclohexyl-2-(phenyl(pyridin-2-yl)methylene)hydrazinecarbothioamide (L4).** Yield 71%. *Anal. Calcd* for $C_{19}H_{22}N_4S$: C, 67.42; H, 6.55; N, 16.55. Found: C, 67.49; H, 6.51; N, 16.50. ^{1}H NMR (600 MHz, DMSO-d_6) δ 12.82 (s, 1H), 8.87 (ddd, J = 4.9, 1.8, 0.9 Hz, 1H), 8.25 (d, J = 8.6 Hz, 1H), 8.02 (td, J = 7.8, 1.9 Hz, 1H), 7.62 (t, J = 1.8 Hz, 1H), 7.62–7.59 (m, 2H), 7.48 (dd, J = 5.0, 2.3 Hz, 2H), 7.34 (dd, J = 8.1, 1.1 Hz, 1H), 4.20–4.16 (m, 1H), 1.88 (dd, J = 12.4, 4.0 Hz, 2H), 1.72 (dt, J = 13.3, 3.5 Hz, 2H), 1.62–1.58 (m, 1H), 1.46 (dd, J = 11.7, 3.5 Hz, 2H), 1.28 (dt, J = 12.9, 3.5 Hz, 2H), 1.20–1.04 (m, 2H). MS m/z (%) 337.16 (M − H, 100).

***N*-Cyclohexyl-*N*-methyl-2-(phenyl(pyridin-2-yl)methylene)-hydrazinecarbothioamide (L6).** Yield 79%. *Anal. Calcd* for $C_{20}H_{24}N_4S$: C, 68.15; H, 6.86; N, 15.89. Found: C, 68.21; H, 6.81; N, 15.85. ^{1}H NMR (600 MHz, DMSO-d_6) δ 13.01 (s, 1H), 8.93–8.86 (m, 1H), 8.06–8.02 (m, 1H), 7.67 (ddt, J = 7.1, 3.7, 1.6 Hz, 2H), 7.65–7.62 (m, 1H), 7.56–7.53 (m, 1H), 7.49 (dd, J = 3.5, 1.4 Hz, 2H), 7.37–7.30 (m, 1H), 3.03 (s, 3H), 1.77 (d, J = 13.1 Hz, 2H), 1.65 (d, J = 12.2 Hz, 2H), 1.59 (s, 1H), 1.47 (dd, J = 12.3, 3.6 Hz, 2H), 1.30 (dt, J = 13.2, 3.4 Hz, 2H), 1.17–1.06 (m, 2H). MS m/z (%) 351.16 (M − H, 100).

Synthesis and characterization of Ga(III) complexes

The synthesis of Ga(III) complexes (**C1–C6**) was performed by previous methods.[11] A solution of thiosemicarbazone in methanol (10 mL, 1 mM) was added $GaCl_3$ (one mole equivalent) with stirring and set still, waiting for the solvent to slowly emanate. After a few days, the Ga(III) complex crystals were obtained and washed with ethanol, followed by vacuum drying.

Dichlorido[2-(phenyl(pyridin-2-yl)methylene)hydrazinecarbothioamide-*N*,*N*′,*S*]gallium(III) (C1). Yield 81%. *Anal. Calcd* for $C_{13}H_{11}Cl_2GaN_4S$: C, 39.43; H, 2.80; N, 14.15. Found: C, 39.50; H, 2.84; N, 14.13. ESI-MS, m/z (r. i.): 392.93 (M − H, 100).

Dichlorido[*N*-methyl-2-(phenyl(pyridin-2-yl)methylene)hydrazinecarbothioamide-*N*,*N*,*S*]-gallium(III) (C2). Yield 85%. *Anal. Calcd* for $C_{14}H_{13}Cl_2GaN_4S$: C, 41.01; H, 3.20; N, 13.67. Found: C, 41.07; H, 3.16; N, 13.69. ESI-MS, m/z (r. i.): 406.95 (M − H, 100).

Dichlorido[*N*-ethyl-2-(phenyl(pyridin-2-yl)methylene)hydrazinecarbothioamide-*N*,*N*,*S*]-gallium(III) (C3). Yield 83%. *Anal. Calcd* for $C_{15}H_{15}Cl_2GaN_4S$: C, 42.49; H, 3.57; N, 13.21. Found: C, 42.43; H, 3.51; N, 13.27. ESI-MS, m/z (r. i.): 420.97 (M − H, 100).

Dichlorido[*N*-cyclohexyl-2-(phenyl(pyridin-2-yl)methylene)-hydrazinecarbothioamide-*N*,*N*,*S*]-gallium(III) (C4). Yield 82%. *Anal. Calcd* for $C_{19}H_{21}Cl_2GaN_4S$: C, 47.73; H, 4.43; N, 11.72. Found: C, 47.76; H, 4.40; N, 11.77. ESI-MS, m/z (r. i.): 475.01 (M − H, 100).

Dichlorido[*N*,*N*-dimethyl-2-(phenyl(pyridin-2-yl)methylene)-hydrazinecarbothioamide-*N*,*N*,*S*]-gallium(III) (C5). Yield 86%. *Anal. Calcd* for $C_{15}H_{15}Cl_2GaN_4S$: C, 42.49; H, 3.57; N, 13.21. Found: C, 42.44; H, 3.52; N, 13.29. EI-MS, m/z (r. i.): 4.6.94 (100), $[M - CH_3]^+$; 387.00 (19.5), $[M - Cl]^+$.

Dichlorido[*N*-cyclohexyl-*N*-methyl-2-(phenyl(pyridin-2-yl)-methylene)hydrazinecarbothioamide-*N*,*N*,*S*]-gallium(III) (C6). Yield 89%. *Anal. Calcd* for $C_{20}H_{23}Cl_2GaN_4S$: C, 48.81; H, 4.71; N, 11.38. Found: C, 48.85; H, 4.75; N, 11.42. EI-MS, m/z (r. i.): 475.01 (100), $[M - CH_3]^+$; 455.06 (31.2), $[M - Cl]^+$; 371.98 (19.5), [M − phenyl]$^+$.

Determination of structure of Ga(III) complexes

The single crystal of **C6** was placed on a glass fiber. The cell constants and crystal data are accurately measured by RAPID IP diffractometer or Rigaku AFC5S (Mo Ka radiation, k = 0.71069 A). The crystal structures were solved directly and differential Fourier calculations were performed, followed by full matrix least squares refinement using the SHELXL97 and TEXSAN package. All non-hydrogen atoms were refined anisotropically. Crystal data, structural refinement and data collection are shown in Table 1.

Cytotoxicity assay (MTT)

The cell lines were cultured in an incubator (ThermoFisher) with 5% CO_2, 95% air at 37 °C. We used a MTT (3-(4,5-dimethyl-2-thiazolyl)-2,5-diphenyl-2-H-tetrazolium bromide) assay to investigate the cell cytotoxicity. Dissolving the thiosemicarbazone ligand and the Ga(III) complex in dimethyl sulfoxide (DMSO) to form a 10 mM stock solution. The DMSO solution in which the complexes were dissolved was diluted with different volumes of cell culture medium to ensure a DMSO concentration of <0.1% so as not to affect cell proliferation. 100 μL of medium containing cells was seeded in 96-well plates and adhered for 12 h at 37 °C, in 5% CO_2/95% air. The seeding densities used were 5×10^4 cells per well. Different concentrations of ligand or Ga(III) complex (20, 10, 5 1, 0.5 μM) were added to the wells and incubated for 48 h, then 20 μL 5 mg mL^{-1} of MTT was added to the wells for another 4 hours. Further added with 100 μL of DMSO, and the optical density (OD) of living cells was measured at a wavelength of 570 nm. The IC_{50} (half maximum inhibitory concentration) values were calculated using the nonlinear multi-purpose curve fitting program (GraphPad Prism).

Cell cycle distribution analysis

HepG-2 cells (5 mL, 1×10^5 cells per mL) were incubated in a 70 mm culture dish, and then the cells were cultured at 37 °C, 5% CO_2/95% air for 12 hours. After treating the cells with **L6** (5 μM) or **C6** (5 μM) for 24 hours, respectively, the collected cells were washed three times with cold phosphate buffer (PBS, pH = 7.4). Cells were immobilized with 75% EtOH for 12 h at −20 °C and washed with iced PBS. The cells were incubated with Ribonuclease (RNase, 2.5 mg mL^{-1}) and stained with 50 mg mL^{-1} propidium iodide for 0.5 hours and analyzed by flow cytometry (BD, Accuri™ C6). Data was analyzed for 10 000 events per sample using MFL 32 software.

Cell apoptosis assay

Apoptosis events in HepG-2 cells induced by **L6** (5 μM) or **C6** (5 μM) were assessed by Annexin V staining and PI according to the procedure of the Detection Kit (Bection Dickinson). We used 2 mL 1×10^6 cells per mL, which were incubated with **L6** (5 μM)

or **C6** (5 μM) for 24 h at 5% CO_2 and 37 °C. HepG-2 cells were dispersed in 300 μL of mixed buffer (140 mM NaCl, pH 7.4, 2.5 mM $CaCl_2$, 10 mM Hepes/NaOH), followed by the addition of 5 μL of PI and Annexin V. Finally, the samples were incubated for 20 minutes at room temperature and assayed by flow cytometry (BD, Accuri™ C6) and analyzed by FlowJo software.

The mitochondrial membrane potential assay

JC-1 (5,5′,6,6′-tetrachloro-1,1′,3,3′-tetraethylbenzimidazolcarbocyanine iodide) staining of mitochondrial membrane potential of HepG-2 cells induced by **L6** (5 μM) or **C6** (5 μM) was performed according to the JC-1 test kit (Biyuntian, Suzhou) method. HepG-2 cells were incubated with **L6** (5 μM) or **C6** (5 μM) for 0.5 hours at 37 °C for 24 h. The cells washed with iced PBS were incubated with 1 μg mL^{-1} of JC-1 for 0.5 h at 37 °C in the dark. After centrifugation, the supernatant was rinsed three times with cold PBS (phosphate buffer, pH = 7.4). Data was obtained by flow cytometry (BD, Accuri™ C6) and FlowJo software was performed to analyze the results.

Intracellular ROS measurements

Evaluation of intracellular ROS was performed by the procedure of active oxygen assay kit (Beyotime, Suzhou) and flow cytometry. Incubate HepG-2 cells with **L6** (5 μM) or **C6** (5 μM) in serum-free cell culture medium for 24 h at 37 °C. 2 μM 2′,7′-dichlorodihydro-fluorescein diacetate (H_2DCF-DA) was added to the cells, and the samples were washed with serum-free medium. Data was obtained by flow cytometry (BD, Accuri™ C6) and FlowJo software was used to analyze the results.

Caspase-3 and caspase-9 activity analysis

The activities of caspase-3 and caspase-9 were detected by CaspGLOW™ Fluorescein Active Caspase-3 and Caspase-9 Staining Kits. **L6** (5 μM) or **C6** (5 μM) was added to HepG-2 cells for 24 hours. The controlled cells were harvested from RPMI 1640 medium containing 10% fetal calf serum (FBS), then centrifuged and washed three times with PBS. The cells were uniformly mixed with 300 mL of the culture broth, followed by the addition of 1 μL of FITC-DEVD-FMK, and the sample was allowed to stand at 37 °C for an hour. Samples were tested on a BD Accuri™ C6 flow cytometer. The experimental results are expressed as a percentage change in activity between the sample and the untreated control.

Western blot analysis

5 mL of HepG-2 cells (1×10^5 cells per mL) were seeded on a 100 mm diameter dish and incubated for 24 h at 37 °C, in 5% CO_2/95% air atmosphere. Cells were harvested and washed 3 times with ice-cold PBS after treatment of **L6** (5 μM) or **C6** (5 μM) for 24 hours. The cells were disrupted with buffer and centrifuged at 10 000*g* for 15 minutes under 4 °C to obtain a supernatant. The protein concentration was determined using a BSA Assay Kit (Beyotime, China), and the samples were detected by SDS-polyacrylamide gel electrophoresis. Under ice bath conditions, the protein was loaded on the polyvinylidene fluoride membrane for 3 hours, followed by preparation of skim milk (5%) for the presence of protein-blocked 1 h in TBST buffer at 25 °C. Membranes and primary antibodies were incubated overnight at 4 °C and washed three times with TBST buffer (20 mM Tris–HCl, 0.05% Tween 20, 150 mM NaCl, pH 8.0). After the membranes were incubated with the secondary antibody for 1 h at 25 °C, they were washed three times in the same manner. Immunoreactivity was imaged by Amersham ECL Plus (Amersham) and the amount of protein in each lane was determined by β-actin.

Statistical analysis

The significance of the differences was assessed by the Student's *t* test. The experimental results are shown as mean ± SD, and when $p < 0.05$, it is indicated that the data is significant.

Conclusions

Herein, we report a series of thiosemicarbazide ligands and gallium complexes with potential antiproliferative activity. The structure–activity relationship results indicate that the modification of the lipophilic group on the ligand significantly improve its antiproliferative activity, and the anti-cancer activity after coordination with gallium is further improved. Ga(III) complex disrupts cellular iron metabolism by up-regulating the expression of TfR1 and down-regulating ferritin. Studies on the apoptosis mechanism of cells show that Ga(III) complex promotes the apoptosis of HepG-2 cells by regulating pro-apoptotic factors (apaf-1, cyt-c and caspase) through the mitochondrial apoptosis pathway. Ligands and gallium complexes inhibit cell cycle distribution by regulating the expression of cyclin-dependent kinases (Cdk 2) and cyclins (cyclin A and cyclin E). The results of the anticancer mechanism indicate that the increased cytotoxicity of the Ga(III) complexes compared with ligands is a result of a combination of multiple mechanisms related to the ability to promote apoptosis and inhibition of cell cycle transition in HepG-2 cells. Overall, these findings are highly beneficial for the development of Ga(III)-thiosemicarbazone complexes as potential anti-cancer therapeutics.

Conflicts of interest

There are no conflicts to declare.

Acknowledgements

This work was supported by National Natural Science Foundation of China (81571812), Pingdingshan College PhD Startup Fund under Grant PXY-BSQD-202003; Key Specialized Research and Development breakthrough in Henan Province (202102310476 and 182102310181); and A Project Funded by the Priority Academic Program Development of Jiangsu Higher Education Institutions under Grant 1107047002.

Notes and references

1 P. Collery, B. Keppler, C. Madoulet and B. Desoize, *Critical Reviews in Oncology/Hematology*, 2002, **42**, 283–296.
2 C. R. Chitambar, *Met. Ions Life Sci.*, 2018, **18**, DOI: 10.1515/9783110470734-016.
3 D. J. Straus, *Semin. Oncol.*, 2003, **30**, 25–33.
4 V. Nikolova, S. Angelova, N. Markova and T. Dudev, *J. Phys. Chem. B*, 2016, **120**, 2241–2248.
5 K. Kumar, S. Schniper, A. González-Sarrías, A. A. Holder, N. Sanders, D. Sullivan, W. L. Jarrett, K. Davis, F. Bai, N. P. Seeram and V. Kumar, *Eur. J. Med. Chem.*, 2014, **86**, 81–86.
6 J. Qi, Q. Yao, K. Qian, L. Tian, Z. Cheng and Y. Wang, *J. Inorg. Biochem.*, 2018, **186**, 42–50.
7 X. Zhang, Y. Jiang and N. Xiao, *Chem. Commun.*, 2018, **54**, 12812–12815.
8 L. Xiao, S. Sun, Z. Pei, Y. Pei, Y. Pang and Y. Xu, *Biosens. Bioelectron.*, 2015, **65**, 166–170.
9 J. A. Lessa, G. L. Parrilha and H. Beraldo, *Inorg. Chim. Acta*, 2012, **393**, 53–63.
10 I. C. Mendes, M. A. Soares, R. G. Dos Santos, C. Pinheiro and H. Beraldo, *Eur. J. Med. Chem.*, 2009, **44**, 1870–1877.
11 J. Qi, Q. Yao, K. Qian, L. Tian, Z. Cheng, D. Yang and Y. Wang, *Eur. J. Med. Chem.*, 2018, **154**, 91–100.
12 A. Mohsen, C. Saby, P. Collery, G. M. Sabry, R. E. Hassan, A. Badawi, P. Jeannesson, D. Desmaële and H. Morjani, *J. Biol. Inorg. Chem.*, 2016, **21**, 837–849.
13 A. Salem, E. Noaman, E. Kandil, A. Badawi and N. Mostafa, *Tumor Biol.*, 2016, **37**, 11025–11038.
14 M. Pribisko, J. Palmer, R. H. Grubbs, H. B. Gray, J. Termini and P. Lim, *Proc. Natl. Acad. Sci. U.S.A.*, 2016, **113**, E2258–E2266.
15 J. Qi, K. Qian, L. Tian, Z. Cheng and Y. Wang, *New J. Chem.*, 2018, **42**, 10226–10233.
16 J. Qi, J. Deng, K. Qian, L. Tian, J. Li, K. He, X. Huang, Z. Cheng, Y. Zheng and Y. Wang, *Eur. J. Med. Chem.*, 2017, **134**, 34–42.
17 J. Qi, Y. Zheng, K. Qian, L. Tian, G. Zhang, Z. Cheng and Y. Wang, *J. Inorg. Biochem.*, 2017, **177**, 110–117.
18 C. R. Chitambar and W. E. Antholine, *Antioxid. Redox sign.*, 2013, **18**, 956–972.
19 J. A. Lessa, M. A. Soares, R. G. Dos Santos, I. C. Mendes, L. B. Salum, H. N. Daghestani, A. D. Andricopulo, B. W. Day, A. Vogt and H. Beraldo, *BioMetals*, 2013, **26**, 151–165.
20 C. R. Kowol, R. Berger, R. Eichinger, A. Roller, M. A. Jakupec, P. P. Schmidt, V. B. Arion and B. K. Keppler, *J. Med. Chem.*, 2007, **50**, 1254–1265.
21 M. Pribisko, J. Palmer, R. H. Grubbs, H. B. Gray, J. Termini and P. Lim, *Proc. Natl. Acad. Sci. U. S. A.*, 2016, **113**, E2258–E2266.
22 C. B. Scarim, D. H. Jornada, M. G. M. Machado, C. M. R. Ferreira, J. L. Dos Santos and M. C. Chung, *Eur. J. Med. Chem.*, 2019, **162**, 378–395.
23 D. B. Lovejoy, D. M. Sharp, N. Seebacher, P. Obeidy, T. Prichard, C. Stefani, M. T. Basha, P. C. Sharpe, P. J. Jansson, D. S. Kalinowski, P. V. Bernhardt and D. R. Richardson, *J. Med. Chem.*, 2012, **55**, 7230–7244.
24 C. Stefani, P. J. Jansson, E. Gutierrez, P. V. Bernhardt, D. R. Richardson and D. S. Kalinowski, *J. Med. Chem.*, 2012, **56**, 357–370.
25 C. R. Kowol, W. Miklos, S. Pfaff, S. Hager, S. Kallus, K. Pelivan, M. Kubanik, É. A. Enyedy, W. Berger, P. Heffeter and B. K. Keppler, *J. Med. Chem.*, 2016, **59**, 6739–6752.
26 J. Kolesar, R. C. Brundage, M. Pomplun, D. Alberti, K. Holen, A. Traynor, P. Ivy and G. Wilding, *Cancer Chemoth. Pharm.*, 2011, **67**, 393–400.
27 É. A. Enyedy, M. F. Primik, C. R. Kowol, V. B. Arion, T. Kiss and B. K. Keppler, *Dalton Trans.*, 2011, **40**, 5895.
28 A. E. Stacy, D. Palanimuthu, P. V. Bernhardt, D. S. Kalinowski, P. J. Jansson and D. R. Richardson, *J. Med. Chem.*, 2016, **59**, 4965–4984.
29 J. G. Da Silva, L. S. Azzolini, S. M. S. V. Wardell, J. L. Wardell and H. Beraldo, *Polyhedron*, 2009, **28**, 2301–2305.
30 J. Loscalzo, *Cell Metab.*, 2008, **8**, 182–183.
31 H. Y. Ryu, J. K. Emberley, J. J. Schlezinger, L. L. Allan, S. Na and D. H. Sherr, *Mol. Pharmacol.*, 2005, **68**, 1087–1096.
32 A. Amsterdam, R. Sasson, I. Keren-Tal, D. Aharoni, A. Dantes, E. Rimon, A. Land, T. Cohen, Y. Dor and L. Hirsh, *Biochem. Pharmacol.*, 2003, **66**, 1355–1362.
33 H. Tuerxun and J. Cui, *Clin. Transl. Oncol.*, 2019, **21**, 695–701.
34 H. S. Chin, M. X. Li, I. Tan, R. L. Ninnis, B. Reljic, K. Scicluna, L. F. Dagley, J. J. Sandow, G. L. Kelly, A. L. Samson, S. Chappaz, S. L. Khaw, C. Chang, A. Morokoff, K. Brinkmann, A. Webb, C. Hockings, C. M. Hall, A. J. Kueh, M. T. Ryan, R. M. Kluck, P. Bouillet, M. J. Herold, D. Gray, D. Huang, M. F. van Delft and G. Dewson, *Nat. Commun.*, 2018, **9**, 4976.
35 Y. Liang, B. Mafuvadze, C. Besch-Williford and S. M. Hyder, *Breast Cancer*, Dove Med Press, 2018, vol. 10, pp. 53–67.
36 H. Han, J. Hemp, L. A. Pace, H. Ouyang, K. Ganesan, J. H. Roh, F. Daldal, S. R. Blanke and R. B. Gennis, *Proc. Natl. Acad. Sci. U. S. A.*, 2011, **108**, 14109–14114.
37 C. Chen, Y. Liu, Y. Liu and P. Zheng, *Cell Cycle*, 2009, **8**, 1158–1160.
38 T. Paul, A. Banerjee, S. Reddy, S. K. Mahato and N. Biswas, *Anticancer Drugs*, 2019, **30**, 167–178.
39 M. D. Ramamoorthy, A. Kumar, M. Ayyavu and K. N. Dhiraviam, *Anticancer Agents Med. Chem.*, 2018, **18**, 1313–1322.
40 D. G. Lee, B. K. Choi, Y. H. Kim, H. S. Oh, S. H. Park, Y. S. Bae and B. S. Kwon, *Cancer Lett.*, 2016, **382**, 186–194.
41 R. Tamura, M. Takada, M. Sakaue, A. Yoshida, S. Ohi, K. Hirano, T. Hayakawa, N. Hirohashi, K. Yura and K. Chiba, *Sci. Rep.*, 2018, **8**, 1611.
42 H. Bardak, A. C. Uguz and Y. Bardak, *Physiol. Int.*, 2017, **104**, 301–315.
43 T. Kanno and T. Nishizaki, *J. Cell. Physiol.*, 2011, **226**, 2329–2337.
44 P. Xia, Y. Liu, J. Chen, S. Coates, D. X. Liu and Z. Cheng, *J. Biol. Chem.*, 2018, **293**, 19672–19685.